PAI-1–regulated miR-21 defines a novel age-associated fibrogenic pathway in muscular dystrophy

Esther Ardite,[1,2] Eusebio Perdiguero,[1,2] Berta Vidal,[1,2] Susana Gutarra,[1,2] Antonio L. Serrano,[1,2] and Pura Muñoz-Cánoves[1,2,3]

[1]Cell Biology Group, Department of Experimental and Health Sciences, Pompeu Fabra University, 08003 Barcelona, Spain
[2]Centro de Investigación Biomédica en Red de Enfermedades Neurodegenerativas, 28031 Madrid, Spain
[3]Institució Catalana de Recerca i Estudis Avançats, 08010 Barcelona, Spain

Disruption of skeletal muscle homeostasis by substitution with fibrotic tissue constitutes the principal cause of death in Duchenne muscular dystrophy (DMD) patients, yet the implicated fibrogenic mechanisms remain poorly understood. This study identifies the extracellular PAI-1/urokinase-type plasminogen activator (uPA) balance as an important regulator of microribonucleic acid (miR)–21 biogenesis, controlling age-associated muscle fibrosis and dystrophy progression. Genetic loss of PAI-1 in mdx dystrophic mice anticipated muscle fibrosis through these sequential mechanisms: the alteration of collagen metabolism by uPA-mediated proteolytic processing of transforming growth factor (TGF)–β in muscle fibroblasts and the activation of miR-21 expression, which inhibited phosphatase and tensin homologue and enhanced AKT signaling, thus endowing TGF-β with a remarkable cell proliferation–promoting potential. Age-associated fibrogenesis and muscle deterioration in mdx mice, as well as exacerbated dystrophy in young PAI-$1^{-/-}$ mdx mice, could be reversed by miR-21 or uPA-selective interference, whereas forced miR-21 overexpression aggravated disease severity. The PAI-1–miR-21 fibrogenic axis also appeared dysregulated in muscle of DMD patients, providing a basis for effectively targeting fibrosis and muscular dystrophies in currently untreatable individuals.

Introduction

Duchenne muscular dystrophy (DMD) remains an incurable genetic disease that primarily affects homeostasis of skeletal muscle, the most abundant tissue of the body, causing its progressive deterioration, paralysis, and premature death. The substitution of muscle by collagenous sclerotic tissue (fibrosis) is a hallmark of DMD, which aggravates disease severity in patients at advanced stages (including the majority of affected individuals). Fibrosis also compromises the efficacy of ongoing preclinical gene- and cell-delivery therapies. No treatment for combating fibrosis in DMD is yet available; neither are the mechanisms underlying fibrosis development in dystrophic muscle well understood. Therefore, their elucidation is critical for attenuating disease progression and for developing improved therapies, especially in individuals of more advanced age.

Mounting evidence indicates a critical involvement of myofiber extrinsic factors in DMD disease progression (Deconinck and Dan, 2007; Serrano and Muñoz-Cánoves, 2010; Zhou and Lu, 2010; Mann et al., 2011). Indeed, both resident and infiltrating cells within the muscle stroma are known to release cytokines and growth factors that may influence muscle homeostasis by controlling degeneration/regeneration, inflammation, and fibrosis (Serrano and Muñoz-Cánoves, 2010). Increased activity of the profibrotic cytokine TGF-β1 in dystrophic muscle of DMD patients and mdx mice (a model of DMD) is associated with an age-dependent alteration of collagen metabolism (Serrano and Muñoz-Cánoves, 2010). Immune neutralization of TGF-β1 in mdx mice reduced the extent of fibrosis (Andreetta et al., 2006), but, unexpectedly, it also resulted

Correspondence to Pura Muñoz-Cánoves: pura.munoz@upf.edu

Abbreviations used in this paper: CTX, cardiotoxin; DMD, Duchenne muscular dystrophy; H/E, hematoxylin/eosin; ISH, in situ hybridization; LNA, locked nucleic acid; miR, microRNA; MMP, matrix metalloproteinase; TA, tibialis anterior; uPA, urokinase-type plasminogen activator; WT, wild type.

The Rockefeller University Press $30.00
J. Cell Biol. Vol. 196 No. 1 163–175
www.jcb.org/cgi/doi/10.1083/jcb.201105013

in an exacerbated inflammatory response with subsequent deleterious effects on muscle repair, thus precluding direct inactivation of TGF-β1 as a therapeutic option for combating fibrosis in DMD. Therefore, it becomes clinically relevant to identify more specific targets within the TGF-β1 profibrotic pathway in dystrophic muscle. TGF-β1 is secreted as a latent protein that is converted to its active form pericellularly by proteolytic processing (mainly via plasmin protease cleavage) and/or by integrin-induced conformational modification (Pedroja et al., 2009; Hayashida, 2010; Worthington et al., 2011). Upon receptor engagement, active TGF-β1 induces a gene expression response through Smad transcription factor–mediated signaling. Smad proteins, in addition to its genomic functions, have recently been shown to be an integral part of the DROSHA processing complex, leading to microRNA (miR)-21 biogenesis and subsequent expression in vitro (Davis et al., 2008). Based on its overexpression in most tumor types analyzed so far, miR-21 is considered an oncomiR (Medina et al., 2010; Pan et al., 2011), although it has also been detected in heart and lung cells after tissue damage (Thum et al., 2008; Liu et al., 2010), suggesting physiopathological functions besides cancer promotion.

Fibroblasts (the major collagen-producing cells) within the stromal tissue microenvironment have an increasingly appreciated role as an autocrine source of profibrotic stimuli (Serrano and Muñoz-Cánoves, 2010) associated with tissue scar formation and fibrosis, but their causal implication in dystrophic muscle progression and the underlying mechanisms remain unclear. In this study, we have investigated the regulatory role of miR-21 in age-associated dystrophic muscle fibrosis and the molecular components of the miR-21–dependent fibrotic pathway in experimentally injured muscle, mdx mice, and DMD patients. We have found that muscle stromal fibroblasts produce proteases, protease inhibitors, and growth factors that trigger and uphold acute and chronic profibrotic conditions, thus altering muscle homeostasis, through stimulation of miR-21 profibrotic actions. We demonstrate an extracellular proteolytic control of miR-21 biogenesis in muscle resident fibroblasts, which, if dysregulated, results in AKT-dependent fibroblast proliferation, altered collagen metabolism, and disease aggravation, with potential clinical implications.

Results

miR-21 drives fibrosis in injured and dystrophic skeletal muscle

To determine whether miR-21 is involved in the development of skeletal muscle fibrosis, we first studied its expression in mouse limb skeletal muscle subjected to laceration, an injury model inducing strong collagen accumulation (fibrosis), as shown by Sirius red staining and biochemical collagen quantification (Fig. 1, A and B) compared with noninjured muscle (Fig. 1 B). Next, we investigated whether miR-21 was also regulated in mdx dystrophic mice by analyzing its expression in diaphragm (the mdx muscle better mimicking human DMD fibrosis development and dystrophy progression). miR-21 expression was induced in mdx diaphragm muscle age dependently compared with age-matched wild-type (WT) muscle (Fig. 1 C), reaching maximal levels around 8 mo of age, correlating with fibrotic outcome (Fig. 1, D and E). Indeed, Sirius red staining and biochemical collagen protein levels were increased in dystrophic diaphragm of mdx mice compared with WT at all ages analyzed (Fig. 1, D and E), reaching a plateau at ∼10–12 mo of age. Moreover, the number of fibroblasts (the major collagen-producing cell type) as well as the expression of ECM homeostasis–related genes such as collagen I and tissue inhibitor of metalloproteinases–1 (TIMP-1) were increased in mdx diaphragms (Fig. 1, F and G). To confirm this correlation, we analyzed miR-21 expression in limb muscles (in which fibrosis is prominent exclusively in aged mice) of young and old mdx mice (Fig. S1, A and B; Stedman et al., 1991). We found that miR-21 expression was robustly increased in gastrocnemius muscle of 24-mo-old mdx mice compared with 3.5-mo-old mice (Fig. S1 C). The expression of miR-21 was principally ascribed to fibroblasts within the fibrotic muscle microenvironment, as revealed by a combination of in situ hybridization (ISH) and immunohistochemistry specific for miR-21 and fibroblasts, respectively (Figs. 1 H and S1 D; Flier et al., 2010; Mathew et al., 2011). Importantly, miR-21 was also found highly expressed in muscle biopsies of DMD patients compared with healthy controls of similar age, correlating with extensive tissue fibrosis (Fig. 1, I and J). Thus, miR-21 expression is specifically dysregulated in skeletal muscle disease. Elevated miR-21 expression in muscle fibroblasts parallels collagen production, both in experimental-induced muscle fibrosis as in muscular dystrophy–associated fibrosis in mouse and humans.

To provide direct evidence for a regulatory role of miR-21 in skeletal muscle fibrosis, WT-lacerated muscles (Fig. 2, A and B) and muscles of aged mice (Fig. 2, C and D) were subjected to an miR-21 modulatory treatment by miR-21 inhibition (antagomiR-21, hereafter referred to as Ant-miR-21) or miR-21 overexpression (Mimic-miR-21) for 1 or 4 wk, respectively. Ant-miR-21 treatment reduced miR-21 expression (but not the expression of an unrelated miR, miR-146) in the muscle of both mouse fibrotic models, whereas delivery of a scrambled oligomiR (Scramble) or a validated point mutant of Ant-miR-21, termed Ant-miR-21 U/C3, had no effect (Figs. 2 [B and D] and S1 [G and H]). Consistent with the blunted miR-21 expression, treatment with Ant-miR-21 (but not with a scrambled oligomiR) prevented the appearance of fibrosis-indicative parameters, such as collagen and fibronectin accumulation and fibroblast number, in lacerated WT muscle (Figs. 2 [A and B] and S1 E), and, more importantly, these fibrotic indicators were also reversed by Ant-miR-21 treatment in limb muscles of 24-mo-old mdx mice (at the stage at which mdx fibrosis is generally considered irreversible; Figs. 2 [C and D] and S1 F). Conversely, the sole overexpression of miR-21 by intramuscular administration of an miR-21 mimic anticipated and exacerbated fibrosis in lacerated muscles of WT mice and in young mdx mice (3 mo old; Fig. 2, A–E). These results demonstrate the efficacy of miR-21 silencing in preventing and treating muscle fibrosis. Notably, miR-21 interference for 1 mo in very old mdx dystrophic mice also reduced muscle deterioration (Fig. 2 F). As affected individuals with prominent fibrosis at advanced disease stages of DMD represent the vast majority

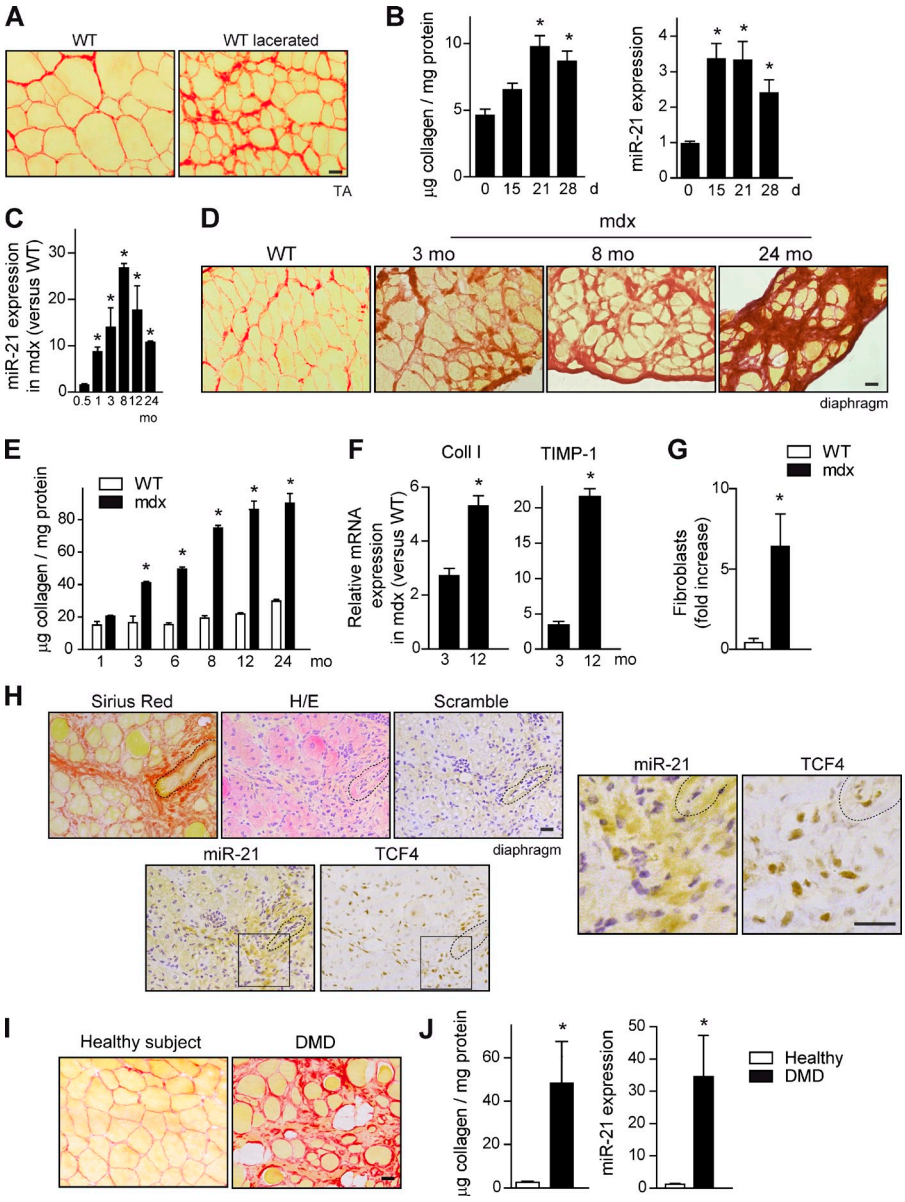

Figure 1. **Dysregulated miR-21 expression in dystrophic muscle of DMD patients and mdx mice is associated with fibrotic outcome.** (A) A representative example of increased collagen deposition (fibrosis), as detected by Sirius red staining of TA muscle of WT mice examined at 21 d after tissue injury induced by laceration. Bar, 25 µm. (B) Quantification of fibrosis (collagen levels) and miR-21 expression in muscles of WT mice before and at the indicated time points after laceration (*, $P < 0.001$ vs. 0 d; means ± SEM; $n = 5$ for each group). (C) miR-21 expression levels were analyzed in the diaphragm muscle of 0.5-, 1-, 3-, 8-, 12-, and 24-mo-old mdx mice by quantitative PCR. mdx mice values were normalized with respect to values of aged-matched WT mice (*, $P < 0.001$ vs. 0.5 mo; means ± SEM; $n = 5$ for each group). (D) A representative example of Sirius red staining of diaphragm muscle sections of 3-mo-old WT mice and of mdx mice at 3, 8, and 24 mo of age. Bar, 25 µm. (E) Collagen content was analyzed in the diaphragm muscle at the indicated ages in mdx and WT mice of the same ages (*, $P < 0.001$ vs. WT; means ± SEM; $n = 4$ for each group). (F) mRNA from diaphragms of mdx mice (and WT mice) of 3 and 12 mo of age was analyzed by quantitative PCR. The expression levels of fibrosis/ECM-related genes, collagen I (Coll I), and TIMP-1 are shown. Results are expressed as fold induction overexpression levels in WT mice (*, $P < 0.01$; means ± SEM; $n = 4$ for each group). (G) Quantification of fibroblasts after detection by immunohistochemistry using antibodies against FSP-1 and TCF-4 in the diaphragm of WT and mdx mice. Data obtained from both markers were averaged and expressed as a fold increase in mdx versus WT muscles (*, $P < 0.001$; means ± SEM; $n = 4$ for each group). (H) Serial sections of mdx diaphragms were subjected to ISH with a specific probe for miR-21 expression or a scrambled control probe (ISH in WT samples is shown in Fig. S1 D), immunostaining using antibodies specific for TCF-4, Sirius red staining for collagen detection, and H/E. A blood vessel is outlined (dashed line) in all pictures as a reference. Squares indicate the insets shown at the right at higher magnifications. Bars, 25 µm. (I) A representative example of Sirius red staining in sections of muscle biopsies from DMD patients and healthy control subjects. Bar, 25 µm. (J) Collagen accumulation and miR-21 expression were analyzed in muscle biopsies of DMD patients and healthy controls (*, $P < 0.01$; means ± SEM; $n = 7$ patients 6–12 yr of age; $n = 6$ healthy 9–15 yr of age).

of patients and no treatment for efficiently reducing muscle fibrosis is yet known, these results undoubtedly have a strong therapeutic potential.

Extracellular proteolytic activation of TGF-β is required for miR-21–dependent collagen accumulation in injured skeletal muscle

TGF-β is considered the major profibrotic cytokine in dystrophic muscle (Andreetta et al., 2006; Vidal et al., 2008; Serrano and Muñoz-Cánoves, 2010). However, attempts to use general inhibitors of TGF-β both in muscular dystrophy as in other pathologies coursing with fibrosis have been relatively unsuccessful, indicating that fibrosis development is a more complex phenomenon than expected (Andreetta et al., 2006; Howell and McAnulty, 2006; Liu et al., 2006; Varga and Pasche, 2009). We have found higher levels of active TGF-β1 and Smad2 (phosphorylated Smad2 [P-Smad2]) in muscle biopsies of DMD patients than in healthy subjects (Fig. 3, A and B), correlating with increased expression of TGF-β target genes related to ECM remodeling and fibrosis (Fig. 3 C); similarly, functional TGF-β signaling augmented age dependently in fibrotic muscles of dystrophic mdx mice compared with age-matched WT controls (Fig. 3, D and E). Thus, we next aimed to identify the downstream cellular effectors as well as the upstream

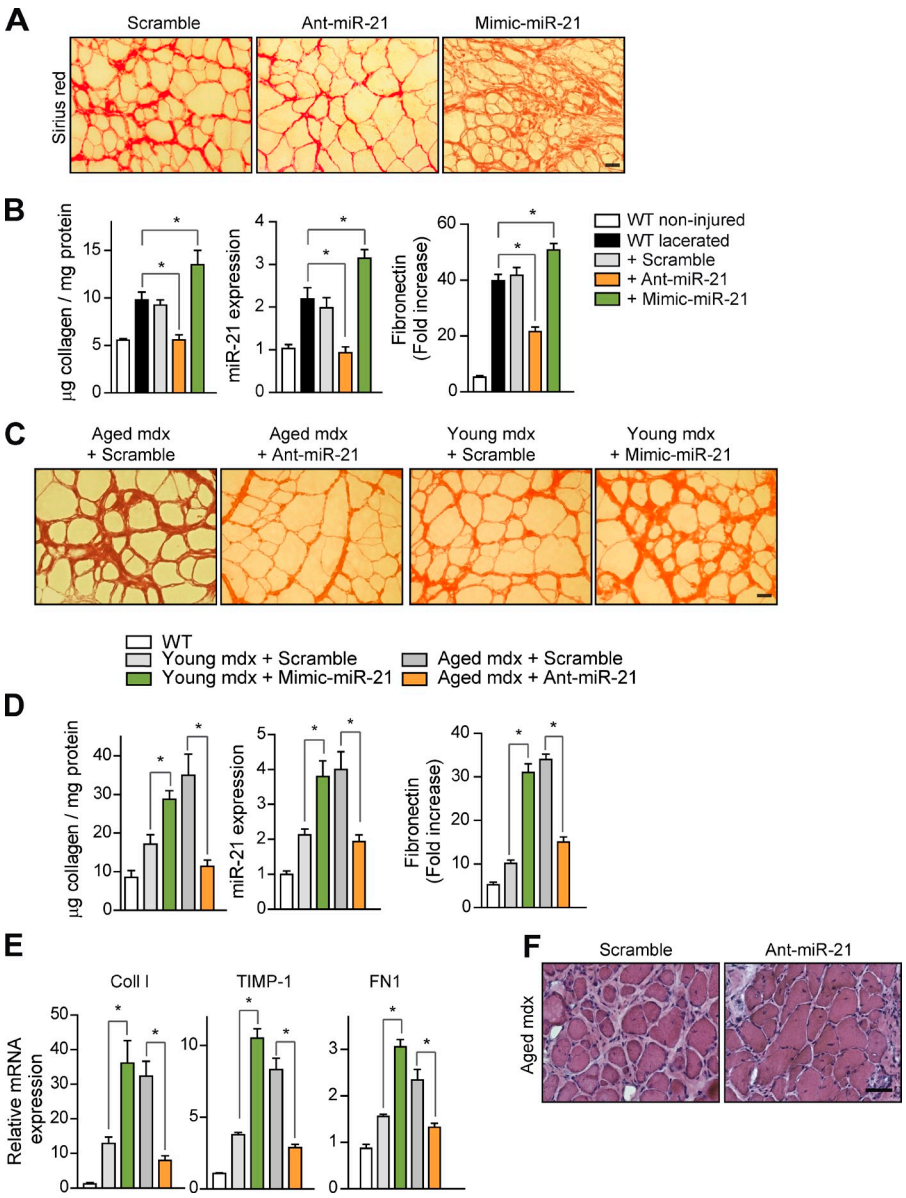

Figure 2. **Efficacy of miR-21 silencing in preventing collagen accumulation after injury and treating muscular dystrophy by reversing fibrosis.** (A) Prevention of fibrosis. TA muscles of WT mice were lacerated, and an antagomir for miR-21 (Ant-miR-21), a mimic for miR-21 (Mimic-miR-21), or Scramble oligomiR (Scramble; used as a negative control) was injected daily for 3 d starting at day 16 after laceration (before significant collagen deposition, which peaks at 21 d), and muscles were collected at day 21 after laceration. Sirius red staining on muscles of treated mice is shown. Bar, 25 µm. (B) Collagen protein accumulation and miR-21 expression were quantified in noninjured and 21-d lacerated muscles of WT mice; similarly, fibronectin was analyzed by immunofluorescence with a specific antibody (see representative panels in Fig. S1 E), and the positively stained areas were quantified by image analysis (*, $P < 0.001$; means ± SEM; $n = 5$ for each group). (C) Therapy for fibrosis. Sirius red staining of gastrocnemius muscle from 24-mo-old mdx mice (aged mdx) after administration of anti–mir-21 (or Scramble) every other day for 1 mo before collection of the muscles (left) and from 3-mo-old mice (young mdx) after administration of Mimic-miR-21 or Scramble with the same protocol (right) is shown. Bar, 25 µm. (D) As in B, collagen accumulation and miR-21 expression were quantified; similarly, fibronectin was analyzed by immunohistochemistry (see representative panels in Fig. S1 F) and quantified (*, $P < 0.001$; means ± SEM; $n = 5$ for each group). (E) The mRNA expression levels of Coll I, TIMP-1, and FN1 in the muscles of mice described in D are shown (*, $P < 0.001$ vs. WT mice; means ± SEM; $n = 5$ for each group). (F) H/E staining of gastrocnemius muscle sections from 24-mo-old mdx mice treated with Ant-miR-21 (or Scramble) for 1 mo. Bar, 50 µm.

extracellular activators of TGF-β in fibrotic muscle using two approaches. Because TGF-β has been shown to induce Smad/DROSHA-mediated miR-21 biogenesis (Davis et al., 2008), in our first approach, we examined whether miR-21 could be a bona fide mediator of TGF-β–dependent fibrogenesis in skeletal muscle and, consequently, a potential better candidate target for fibrosis intervention in muscular dystrophy. As miR-21 is expressed predominantly by fibroblasts within fibrotic areas of mdx diaphragm (Fig. 1 H), we isolated primary fibroblasts from mdx diaphragm and tested miR-21 regulatory function in response to TGF-β1 in vitro. Treatment with TGF-β1 induced mature miR-21 expression in primary muscle fibroblasts (Fig. 3 F), whereas the capacity of these cells to produce TGF-β–dependent fibrosis-associated gene products such as collagen or TIMP-1 was abrogated by transfection with Ant-miR-21 but not a scrambled oligomiR (Fig. 3 G). Furthermore, overexpression of miR-21 by transfection with the Mimic-miR-21 in primary muscle fibroblasts was able to induce the expression of fibrosis-associated genes in the absence of TGF-β1 treatment (Fig. 3 G), demonstrating that miR-21 is a specific regulator of muscle fibroblasts functions, downstream of TGF-β. Consistent with these in vitro results, in vivo delivery of active TGF-β1 to injured WT mouse muscle increased collagen deposition and miR-21 expression compared with vehicle-treated injured muscles (Fig. S1, I and J), whereas antagomiR-21 (but not Scramble) treatment could revert the exacerbated fibrosis in response to TGF-β1 (Fig. S1 J), thus establishing miR-21 as an essential intracellular effector of TGF-β–induced skeletal muscle fibrosis in vitro and in vivo.

In a second approach, we investigated whether the fibrotic muscle had functional mechanisms operating upstream of active TGF-β/miR-21. Because extracellular urokinase-type plasminogen activator (uPA)–dependent plasmin proteolysis is a recognized pathway for conversion of latent TGF-β into its active form in vitro (Yee et al., 1993; Odekon et al., 1994; Nunes et al., 1995; George et al., 2005) and as our previous studies have

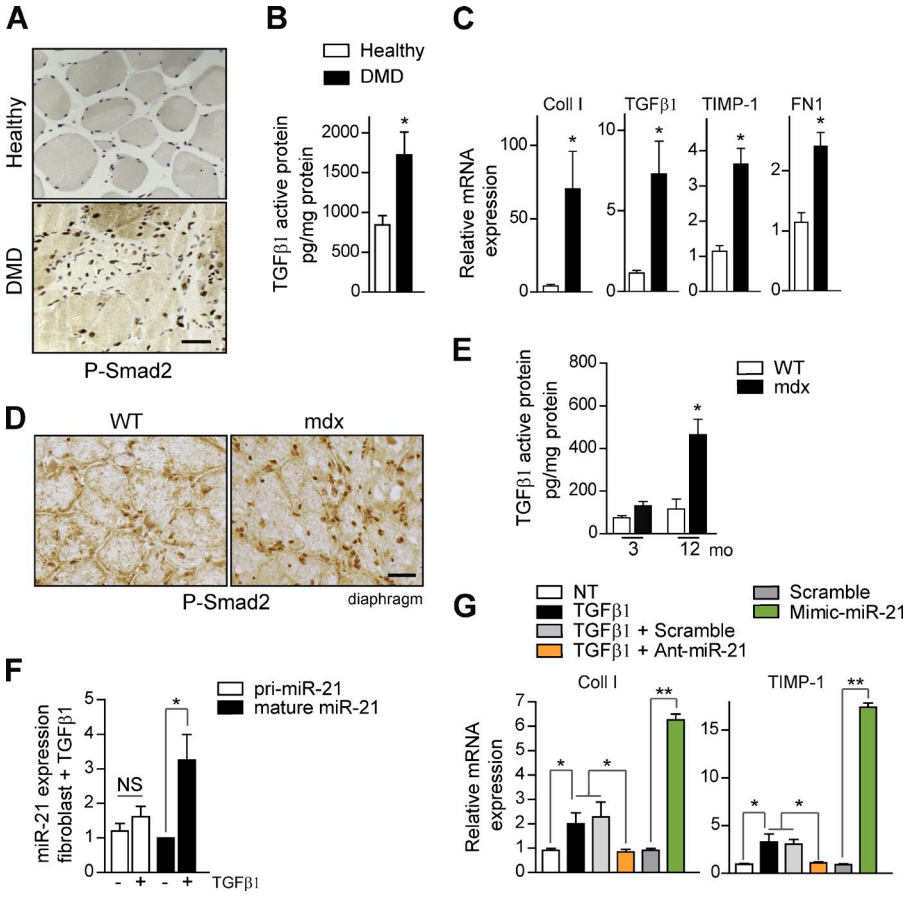

Figure 3. **Increased TGF-β activity regulates miR-21 expression and fibrosis in dystrophic muscle of DMD patients, mdx mice, and in injured WT muscle.** (A) Representative immunostaining of muscle biopsies of DMD patients and healthy control subjects using an anti–P-Smad2 antibody. Bar, 25 µm. (B) Active TGF-β1 protein quantification by ELISA in muscle biopsies of DMD patients and healthy controls. (C) The expression levels of Coll I, TGF-β1, TIMP-1, and FN1 from the same human muscle biopsies used in B are shown. (B and C) *, $P < 0.01$; means ± SEM. $n = 7$ patients 6–12 yr of age; $n = 6$ healthy 9–15 yr of age. (D) Representative immunostaining of diaphragms of WT and mdx mice of 3 mo of age using anti–P-Smad2 antibody. Bar, 25 µm. (E) Active TGF-β1 protein quantification by ELISA in the diaphragm muscle of WT and mdx mice of the indicated age (*, $P < 0.01$; means ± SEM; $n = 4$ for each group). (F) Fibroblasts obtained from skeletal muscle were cultured in vitro and treated with TGF-β1 for 18 h, and the expression of miR-21 and its polyadenylated precursor (Pri-miR-21) was analyzed by quantitative PCR (*, $P < 0.05$; means ± SEM; $n = 5$ for each group). (G) Muscle fibroblasts were left untreated (NT) or were treated with the indicated combinations of TGF-β1 (24 h), Ant-miR-21, Mimic-miR-21, or Scramble oligomiR. The expression of Coll I and TIMP-1 was analyzed by quantitative PCR (*, $P < 0.01$; **, $P < 0.001$; means ± SEM; $n = 4$ for each group).

established the uPA/plasmin system (also known as fibrinolytic system) as an important regulator of skeletal muscle homeostasis after damage (Lluís et al., 2001; Suelves et al., 2002, 2005, 2007), we postulated that this extracellular proteolytic balance might regulate TGF-β activation and profibrogenic actions in fibrotic muscle. To address this question, we used mice deficient in uPA ($uPA^{-/-}$) and its physiological inhibitor PAI-1 ($PAI\text{-}1^{-/-}$) and analyzed uPA/plasmin and TGF-β activation, as well as collagen accumulation and miR-21 expression, in lacerated muscles of the distinct mouse genotypes (Fig. 4, A–C). Compared with noninjured muscle, lacerated muscle of WT mice contained elevated uPA and plasmin activities, as assessed using specific chromogenic substrates for each protease (Fig. S2 A), which were further incremented by PAI-1 loss, whereas these activities were basically abrogated in $uPA^{-/-}$-lacerated muscles, respectively (Fig. S2 A). Activation of TGF-β1 in lacerated muscles was regulated in a uPA/plasmin-dependent manner, as maximal levels of active TGF-β1 and P-Smad2 proteins and downstream ECM remodeling– and fibrosis-associated genes were found in lacerated muscles of $PAI\text{-}1^{-/-}$ mice compared with WT and $uPA^{-/-}$-lacerated muscles, respectively (Figs. 4 [D and E] and S2 [B and C]). Importantly, total levels of TGF-β1 protein and RNA were similar in lacerated muscles of all mouse genotypes, as revealed by a combination ELISA and quantitative PCR (Fig. S2 B and not depicted). Moreover, fibroblasts from PAI-1–deficient muscle, but not WT, showed an unscheduled production of active uPA, TGF-β1, and miR-21 in basal culture conditions (Fig. S2 D), suggesting that PAI-1 prevents excessive proteolytic activation of TGF-β1 and subsequent miR-21 expression in stromal fibroblast cells within injured muscle. Interestingly, latent TGF-β1 can also be activated in certain cell types through integrin-induced conformational changes in vitro (Ludbrook et al., 2003; Pedroja et al., 2009; Hayashida, 2010; Worthington et al., 2011). We found that RGD delivery (a cyclic peptide that specifically interferes with integrin binding to ligand RGD motif) did not significantly affect fibrosis development in lacerated $PAI\text{-}1^{-/-}$ muscles (Fig. S2 E), supporting that, in damaged muscle, PAI-1 expression may serve to restrict the uPA-mediated TGF-β1 activation– and miR-21–driven fibrosis pathway and, hence, muscle disease progression.

Dysregulated miR-21 expression advances fibrosis and myodystrophy in young $PAI\text{-}1^{-/-}$ mdx mice

From a biomedical perspective, it was relevant to investigate whether PAI-1–regulated miR-21 gene expression might be operative in a fibrotic muscle disease context. Accordingly, mdx mice were intercrossed with $PAI\text{-}1^{-/-}$ mice, and $PAI\text{-}1^{+/+}$ mdx and $PAI\text{-}1^{-/-}$ mdx littermates were analyzed at distinct ages. Neither genotype showed any sign of muscle dystrophy by 2 wk of age (before disease onset; unpublished data). However, $PAI\text{-}1^{-/-}$ mdx mice showed an enhanced (and anticipated) collagen deposition in the diaphragm early after disease onset

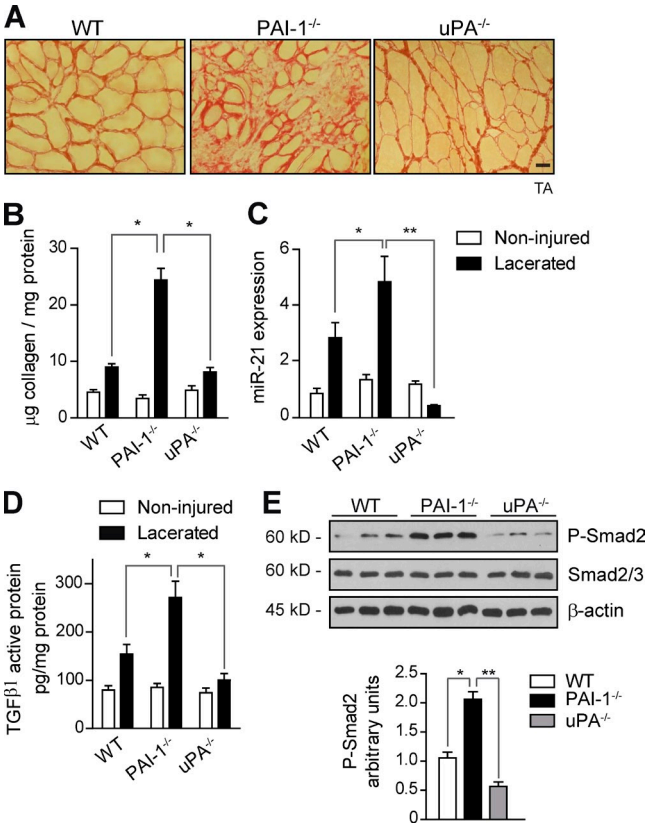

Figure 4. **Lacerated muscles of PAI-1–deficient mice have an exacerbated fibrogenesis with increased TGF-β1 activation, miR-21 expression, and collagen deposition.** (A) Muscle injury was performed by laceration in the TA muscles of WT mice as well as in PAI-1$^{-/-}$, uPA$^{-/-}$, and uPA$^{+/-}$ mice. A representative example of Sirius red staining of muscle sections at 21 d after laceration of the distinct genotypes is shown. Bar, 25 µm. (B) The extent of collagen deposition was quantified in lacerated muscles of all mouse genotypes (*, $P < 0.01$; means ± SEM; $n = 5$ for each group). (C) Analysis of miR-21 expression by quantitative PCR in muscles of mice of the indicated genotypes (*, $P < 0.05$; **, $P < 001$; means ± SEM; $n = 4$ for each group). (D) Active TGF-β1 protein quantification by ELISA in muscles of the same genotypes (*, $P < 0.05$; means ± SEM; $n = 6$ for each group). (E) Extracts of PAI-1$^{-/-}$ and uPA$^{-/-}$-lacerated muscles were analyzed by Western blotting for P-Smad2, total Smad2/3 protein, and β-actin. Quantification of P-Smad2 versus total Smad2/3 and normalized for β-actin levels is shown (*, $P < 0.05$; **, $P < 0.01$; means ± SEM; $n = 7$ for each group).

(i.e., 2.5 and 3.5 mo) compared with age-matched PAI-1$^{+/+}$ mdx mice (Fig. 5 A, closed vs. open symbols), coinciding with increased expression of ECM/fibrosis-associated markers (Fig. 5 B). In fact, pronounced muscle fibrosis was advanced ∼4 mo in young mdx mice lacking PAI-1 (compare 3.5- with 8-mo values in Fig. 5 A; Fig. 5 D), which also presented increased deterioration of muscle tissue structure (Fig. S3 A). Furthermore, physical performance was significantly decreased in PAI-1$^{-/-}$ mdx mice compared with PAI-1$^{+/+}$ mdx mice both at 3.5 and 8 mo of age (Fig. S3, B and C), whereas levels of serum creatine kinase, an indicator of muscle damage, were higher in the former genotype (Fig. 5 C). These findings provide histological, biochemical, and functional evidence that genetic loss of PAI-1 advances the onset of fibrosis and exacerbates disease progression in dystrophic muscle, mimicking the aged dystrophic environment. Interestingly, the maximal levels of fibrosis reached in diaphragm of aged mdx mice (Fig. 1, D and E) coincided with a decrease in PAI-1 expression (compare PAI-1 levels in 3.5- and 12-mo-old mdx diaphragm; Fig. 5 E).

Notably, diaphragms of young PAI-1$^{-/-}$ mdx mice also exhibited augmented levels of active TGF-β1 (but not of total TGF-β1 protein) compared with age-matched PAI-1$^{+/+}$ mdx muscle (Figs. 5 F and S3 D), supporting an increased processing of the latent TGF-β1 protein, rather than de novo growth factor expression, in the absence of PAI-1. Consistent with this, P-Smad2 and miR-21 levels were further increased in PAI-1$^{-/-}$ mdx muscle compared with PAI-1$^{+/+}$ mdx (Fig. 5, F and G). Notably, the exaggerated levels of these fibrotic signaling parameters and the functional deterioration of PAI-1$^{-/-}$ mdx muscle could be significantly reversed by pharmacological and genetic inhibition of uPA using amiloride (a specific uPA inhibitor) and a specific siRNA for uPA (siRNA uPA), respectively (Figs. 5 [D and H] and S3 E). Indeed, siRNA uPA delivery to 3-mo-old PAI-1$^{-/-}$ mdx limb muscle for 3 wk could reduce active TGF-β1 (but not of total TGF-β1 protein), Smad2 activation, and miR-21 expression while lowering collagen deposition (Figs. 5 H and S3 F), which is in agreement with similar beneficial effects of amiloride treatment on the diaphragm of PAI-1$^{-/-}$ mdx mice (Fig. S3 E). Notably, delivery of the RGD peptide could not reduce the exacerbated TGF-β1 activation, miR-21 expression, and fibrosis in PAI-1$^{-/-}$ mdx muscle (Fig. S3 G). Of clinical relevance, we found that treatment of severely dystrophic muscles of very aged mdx mice (24 mo old), which express very low levels of PAI-1, with siRNA uPA was capable of reducing persistent TGF-β1 activation, miR-21 expression, and, more importantly, fibrosis (Fig. 5 I) while improving muscle fitness and recovery (Figs. 5 J and S3 H), and this beneficial effect was comparable with that of anti–miR-21 treatment (Fig. 2, C and D). Reinforcing the existence of an extracellular-regulated fibrotic pathway in the dystrophic muscle microenvironment, we found that siRNA uPA administration could reverse the exacerbated collagen deposition, TGF-β1–induced Smad2 activity, and miR-21 expression in lacerated muscles of PAI-1$^{-/-}$ mice (Fig. S4, A–C). One prediction of these results is that loss of uPA function in mdx mice should result in reduced fibrosis. This is, in fact, observed in 4-mo-old uPA$^{-/-}$ mdx mice, despite the exacerbated degeneration of mdx mice in the absence of uPA (unpublished data; Suelves et al., 2007). Together, these data suggest that a certain level of pericellular PAI-1 is needed to avoid rapid fibrosis progression in injured and dystrophic muscle. Complete loss of PAI-1 results in unrestricted activation of uPA/plasmin in damaged and dystrophic muscle, leading to the unscheduled accumulation of collagen and fibrosis. More importantly, our results show that fibrosis in aged mdx mice, despite being considered irreversible, can be attenuated by specific miR-21 (or uPA) genetic–interfering treatments, improving muscle homeostasis, with potential clinical implications for DMD patients at advanced fibrotic stages.

PAI-1 loss-dependent miR-21 expression induces muscle fibroblast proliferation through promotion of the AKT pathway

As fibroblasts (the major collagen-producing cell type) in dystrophic muscle express miR-21 and also express PAI-1 (Fig. S4 D),

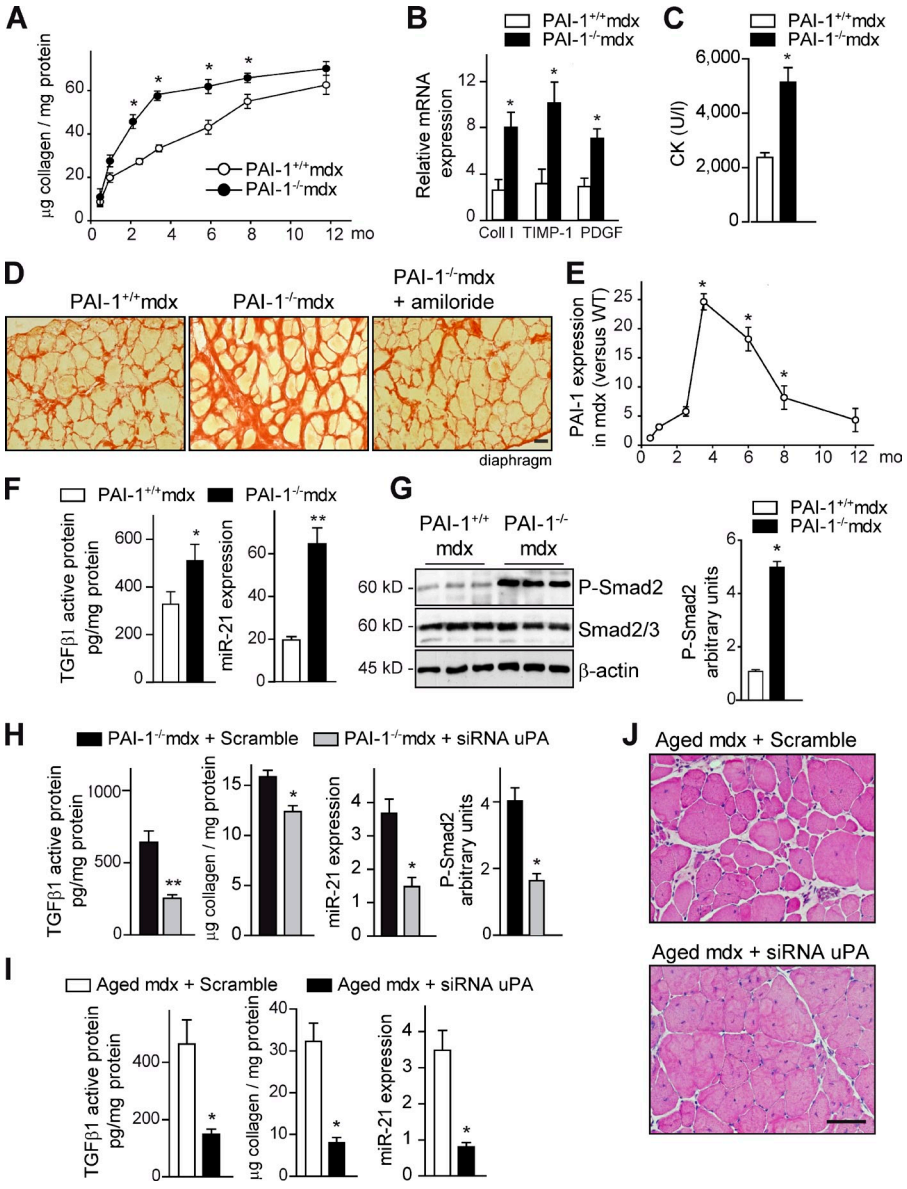

Figure 5. **PAI-1 loss anticipates fibrosis and exacerbates muscle disease progression: Reversal by pharmacological and genetic interference with uPA in vivo.** (A) Fibrosis quantification in diaphragms of PAI-$1^{+/+}$ and PAI-$1^{-/-}$ mdx mice over time (*, $P < 0.01$ vs. age-matched PAI-$1^{+/+}$ mdx; means ± SEM; $n = 5$ for each group). (B) Quantitative PCR analysis of fibrosis-associated markers in diaphragm muscles of 3-mo-old PAI-$1^{+/+}$ and PAI-$1^{-/-}$ mdx mice (*, $P < 0.05$ vs. PAI-$1^{+/+}$ mdx; means ± SEM; $n = 5$ for each group). (C) As in B, serum creatine kinase (CK) levels are shown (*, $P < 0.01$; means ± SEM; $n = 5$ for each group). (D) Representative Sirius red staining in diaphragm muscle sections of 3.5-mo-old PAI-$1^{+/+}$ and PAI-$1^{-/-}$ mdx mice and PAI-$1^{-/-}$ mdx mice treated with amiloride (a uPA inhibitor; see Fig. S3 for additional information). Bar, 25 µm. (E) Quantitative PCR analysis of PAI-1 expression in diaphragm muscle of mdx mice at the indicated ages; values are expressed as fold induction over WT (*, $P < 0.01$ vs. 1 mo; means ± SEM; $n = 5$ for each group). (F) Increased TGF-β1 active protein and miR-21 expression in the diaphragm muscle of PAI-$1^{-/-}$ mdx mice compared with PAI-$1^{+/+}$ mdx mice, as measured by ELISA and quantitative PCR, respectively (*, $P < 0.05$; **, $P < 001$, means ± SEM; $n = 4$ for each group). (G, left) As in F, muscle samples were analyzed by Western blotting using antibodies against the proteins P-Smad2, total Smad2/3, and β-actin. (right) Quantification of P-Smad2 versus total Smad2/3 and normalized for β-actin levels is shown (*, $P < 0.01$; means ± SEM; $n = 5$ for each group). P-Smad2 levels in basal muscle of WT and PAI-$1^{-/-}$ mice were undistinguishable (not depicted). (H) siRNA for uPA or a scrambled control oligomiR was delivered into gastrocnemius muscles of 3-mo-old PAI-$1^{-/-}$ mdx mice every other day for 3 wk, and, after the treatment, muscles were analyzed for TGF-β1 active protein levels, collagen content, miR-21 expression, and Smad2 activity (P-Smad2; *, $P < 0.05$; **, $P < 001$, means ± SEM; $n = 4$ for each group). (I) siRNA for uPA or Scramble was delivered into the gastrocnemius muscle of 24-mo-old mdx mice every other day for an additional 1 mo. Then, muscles were analyzed for TGF-β1 activity, collagen content, and miR-21 expression (*, $P < 0.01$; means ± SEM; $n = 5$ for each group). (J) As in I, H/E staining is shown. Bar, 50 µm.

we postulated that this signaling axis might regulate the fibrogenic functions of muscle fibroblasts. Accordingly, primary fibroblasts were obtained from PAI-$1^{+/+}$ and PAI-$1^{-/-}$ mdx muscle and analyzed in vitro. As previously mentioned, in the absence of profibrotic stimuli, PAI-1–deficient muscle fibroblasts exhibited significant levels of active uPA and TGF-β1, as well as miR-21, compared with PAI-$1^{+/+}$ cells (Fig. S2 D); notably, addition of recombinant PAI-1 (rPAI-1) or interference with uPA using amiloride or siRNA uPA in PAI-1–deficient cells reversed the enhanced fibrogenic activities, whereas scrambled siRNA or the RGD peptide (not depicted) treatments had no effect (Figs. 6 A and S5 B). This indicated that muscle fibroblasts lacking PAI-1 are activated before schedule via autocrine uPA/TGF-β1 secretion and activation, although additional proteolytic TGF-β1–activating pathways cannot be discarded. Unexpectedly, we found that PAI-1–deficient muscle fibroblasts had an enhanced proliferation rate in vitro in response to profibrotic stimuli (TGF-β1; Fig. 6 B), and this was in agreement with the increased presence of fibroblasts in PAI-$1^{-/-}$ mdx muscle compared with PAI-$1^{+/+}$ mdx (Fig. S4 E), indicating that loss of muscle fibroblast–intrinsic PAI-1 endows TGF-β1 with an atypical growth-promoting action, which correlated with an increase in miR-21 expression (Fig. S5 A). Delivery of Ant-miR-21 (but not a scrambled oligomiR) into PAI-$1^{-/-}$ fibroblasts could revert TGF-β1–induced cell proliferation to PAI-$1^{+/+}$ levels (Fig. 6 B) and down-regulated collagen and TIMP-1 expression (Fig. 6 C). These findings unveil PAI-1 as an important extracellular regulator of collagen metabolism in skeletal muscle fibroblasts via miR-21 action.

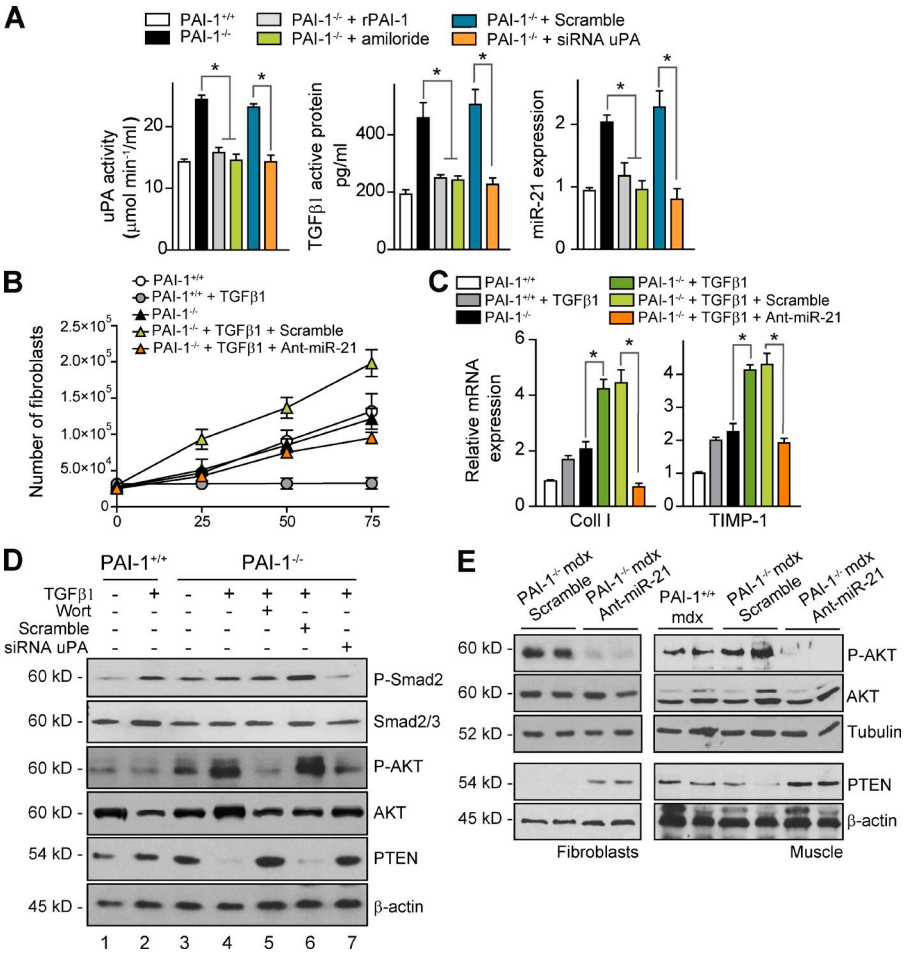

Figure 6. **PAI-1 loss results in dysregulated miR-21 expression, which promotes AKT-mediated cell proliferation of skeletal muscle fibroblasts.** (A) uPA activity (chromogenic assay), active TGF-β1 (ELISA), active TGF-β1 protein, and miR-21 expression (quantitative PCR) were analyzed in muscle fibroblasts from PAI-$1^{+/+}$ and PAI-$1^{-/-}$ mice, either untreated or treated with recombinant PAI-1 (rPAI-1) and amiloride or transfected with siRNA for uPA or Scramble control, as indicated (*, $P < 0.05$; means ± SEM; $n = 4$ for each group). (B) PAI-$1^{+/+}$ and PAI-$1^{-/-}$ muscle fibroblasts, transfected with Ant-miR-21 or Scramble oligomiR, were stimulated or not with 10 ng/ml TGF-β1, and the number of cells was counted at the indicated time points (means ± SEM; $n = 4$ for each group). (C) PAI-$1^{+/+}$ and PAI-$1^{-/-}$ muscle fibroblasts, stimulated as in B, were analyzed for Coll I and TIMP-1 expression after TGF-β1 treatment (*, $P < 0.05$; means ± SEM; $n = 4$ for each group). (D) Extracts of PAI-$1^{+/+}$ and PAI-$1^{-/-}$ muscle fibroblasts, stimulated or not with TGF-β1 for 24 h, were analyzed by Western blotting using antibodies for the proteins P-Smad2, total Smad2/3 protein, P-AKT, total AKT protein, PTEN, and β-actin; in lane 5, PAI-$1^{-/-}$ muscle fibroblasts were incubated with 2 μM wortmannin (Wort) 30 min before the addition of TGF-β1. In lanes 6 and 7, PAI-$1^{-/-}$ muscle fibroblasts were transfected with Scramble and siRNA uPA oligomiRs, respectively, before the addition of TGF-β1. (E) Western blotting analysis of muscle fibroblasts (left) or extracts of gastrocnemius muscles from 3-mo-old PAI-$1^{+/+}$ and PAI-$1^{-/-}$ mdx mice (right) treated every other day for 1 mo with a scrambled oligomiR or Ant-miR-21 using antibodies for the proteins P-AKT, total AKT, PTEN, and β-actin.

To mechanistically understand how PAI-1 loss–driven miR-21 expression regulates fibroblast proliferation in response to TGF-β1, we evaluated the expression of potential miR-21 bona fide targets in PAI-$1^{+/+}$ and PAI-$1^{-/-}$ cells. Among several targets examined, we found phosphatase and tensin homologue (PTEN) levels clearly dysregulated in TGF-β1–stimulated PAI-1–deficient muscle fibroblasts, and, notably, this resulted in activation of AKT, a major signaling mediator of cell metabolic functions affecting proliferation and/or survival (Fig. 6 D, lane 4), suggesting that unbalanced PTEN/AKT signaling may cause hyperproliferation of PAI-$1^{-/-}$ muscle fibroblasts. Accordingly, preincubation of these cells with the AKT pathway inhibitor wortmannin (Fig. 6 D, lane 5) prevented their proliferation in response to TGF-β1 (Fig. S5 C). Importantly, treatment with siRNA uPA rescued the increased activation of TGF-β1 and AKT pathways (Fig. 6 D, lane 7), and treatment with Ant-miR-21 restored PTEN/AKT dysregulation in muscle fibroblasts (Fig. 6 E, left). Consistent with these in vitro results, AKT activation was increased, whereas PTEN levels were reduced, in muscles of PAI-$1^{-/-}$ mdx mice compared with PAI-$1^{+/+}$ mdx mice (Figs. 6 E and S5 D), which is in agreement with the increased fibroblast number and collagen deposition (Figs. 5 [A and D] and S4 E). Of note, genetic in vivo interference with miR-21 and uPA in lacerated muscles of PAI-$1^{-/-}$ mice, besides attenuating the exacerbated fibrogenic features in the absence of PAI-1 (Figs. 6 [B and C] and S3 E), also rescued AKT activation (Figs. 6 E and S5 D) and improved muscle recovery (Fig. S5 E), suggesting detrimental actions for muscle homeostasis by miR-21 and uPA dysregulation. Thus, these results reinforce the conclusion that the extracellular uPA/PAI-1 proteolytic balance is an important upstream regulator of the velocity of fibrosis establishment in dystrophic muscle through controlling miR-21 expression levels. We propose that aberrant PAI-1 loss–induced uPA/plasmin activation could initiate an autocrine loop of TGF-β1 activity in muscle fibroblasts, leading to miR-21–driven fibrogenic activities in dystrophic muscle, thereby aggravating disease progression.

Discussion

Fibrosis development by dysregulated collagen metabolism in DMD patients leads to the derangement of muscle structure and irreversible loss of normal tissue function. In addition, it represents a major obstacle for the success of ongoing preclinical therapies at advanced stages of DMD (which include the vast majority of patients). However, no successful treatment for reducing fibrosis in this disease is yet available. A fundamental unanswered question is the nature of the cellular and molecular mechanisms that lead to persistent fibrotic responses and dystrophic disease aggravation with aging. Hence, their identification may open new therapeutic venues in DMD.

Here, we have characterized a new age-associated fibrogenic regulatory axis in dystrophic and injury-induced skeletal muscle fibrosis in mouse models. In both cases, the expression of miR-21, which is barely detected in normal muscle, increased concomitantly with age-dependent fibrogenesis, whereas the expression of the extracellular proteolytic inhibitor PAI-1 followed an inverse pattern with age. Genetic loss of PAI-1 advanced muscle fibrosis in young dystrophic mice, which could be prevented by direct interference with miR-21 and with the PAI-1 substrate uPA. Consistent with this, overexpression of miR-21 in muscles of young mdx mice sufficed to anticipate fibrosis and enhanced disease severity. Conversely, treatment of senescent mdx mice with an inhibitor of miR-21 reduced fibrosis, which is classically considered irreversible at advanced ages, and improved muscle homeostasis. The relevance of our data is further supported by the finding that miR-21 expression also appeared to be positively associated with muscle fibrosis and disease course in DMD patients.

A critical question is precisely how miR-21 is regulated and how, in turn, it regulates the progression of muscle disease–associated fibrosis. First, we found that the pericellular unbalance of uPA/PAI-1 proteolytic activity in mdx muscle stromal fibroblasts induced the conversion of latent into active TGF-β, resulting in miR-21 expression in these cells, likely through the well-documented DROSHA–Smad interaction, driving miR-21 biogenesis (Davis et al., 2008). In this regard, PAI-1 loss in injured and dystrophic muscle affected several mechanisms (Fig. 7). Fibroblasts in acutely damaged and young dystrophic muscle produce high levels of PAI-1 to tightly control uPA and plasmin activities, thereby preventing exaggerated conversion of pro–TGF-β into its active form and excessive collagen production, hence slowing the advancement of fibrosis in the first months after disease onset. Our results sustain that fibroblast-produced PAI-1 serves as a brake for TGF-β–mediated fibrosis in mdx muscle and highlight the relevance of maintaining uPA/PAI-1 homeostasis to attenuate disease severity in muscular dystrophy. A prediction of this model is that blocking uPA in muscular dystrophy should prevent fibrosis. Indeed, pharmacological and genetic interference with uPA in injured and dystrophic muscle attenuated fibrotic outcome and disease progression in vivo and collagen production by fibroblasts in vitro. As PAI-1 is a TGF-β–inducible gene, increased PAI-1 expression in mdx fibroblasts may provide a negative feedback loop to restrain TGF-β profibrotic actions through neutralizing uPA, thus supporting tissue homeostasis. Our results also prove that, through autocrine uPA-induced TGF-β activation, PAI-1–deficient fibroblasts undergo a hyperproliferative response mediated by persistent activation of the cell proliferation/survival AKT pathway, which is caused by miR-21–mediated PTEN inhibition. Exacerbation of this response via PAI-1 gene loss or via miR-21 overexpression may largely explain the increased number of fibroblasts present in the diaphragm of young PAI-1$^{-/-}$ mdx mice, correlating with increased fibrosis. Our data do not exclude other PAI-1–mediated effects such as uPA-mediated promotion of inflammatory cell infiltrates (Suelves et al., 2007) independent from PAI-1–regulated miR-21 effects in fibroblasts or additional miR-21

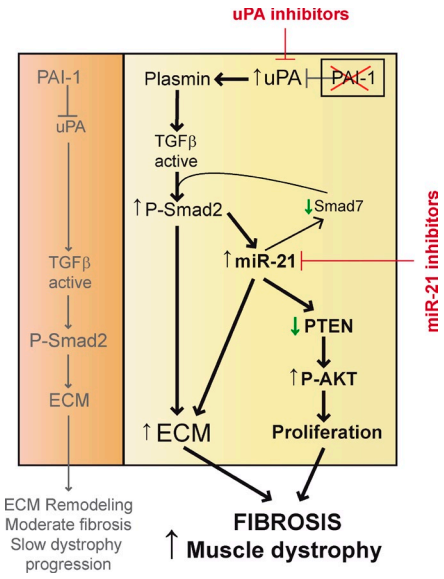

Figure 7. **Proposed mechanisms underlying the regulatory control of fibrosis development by the PAI-1/uPA balance in aged-associated muscle dystrophy progression.** PAI-1 is the physiological inhibitor of the protease uPA, which, through the generation of active plasmin, processes latent TGF-β into its active form. (left) When PAI-1 levels are high (at early stages of dystrophic disease), there is a controlled activation of uPA and production of active TGF-β, which stimulates collagen and TIMP-1 expression in fibroblasts through Smad2-mediated transcriptional activation, thus resulting in altered ECM metabolism and slow development of fibrosis and muscle dystrophy progression. (right) When PAI-1 levels are low (at advanced stages of dystrophic disease), there is a hyperactivation of uPA, leading to increased production of active TGF-β and Smad2 signaling (yet, additional proteolytic TGF-β–activating pathways in fibrotic muscle cannot be discarded). Most importantly, there is a derepression of fibroblast AKT signaling and abnormal fibroblast proliferation through miR-21 (via TGF-β–dependent miR-21 biogenesis), which inhibits the expression of PTEN phosphatase, an inhibitor of AKT activation. The increase in AKT activity results in enhanced muscle fibroblast proliferation, which in turn causes further fibrosis and worsens muscle dystrophy. Interestingly, high miR-21 expression in dystrophic muscle also leads to Smad7 (an inhibitory Smad) down-regulation, thus providing a TGF-β activity–amplifying loop, resulting in increased fibrosis. Whether other additional mechanisms of miR-21 activation, in addition to TGF-β, are operational in this context awaits further investigation. Overall, our data validate uPA as a disease target in muscular dystrophy (as demonstrated by the efficacy of amiloride and genetic uPA interference) and introduces miR-21 as a novel therapeutic candidate.

potential effects in other cell types. It is worth noting that matrix matalloproteinases (MMPs) could also play an obvious role in dystrophic muscle fibrosis, as collagen accumulates when its rate of synthesis is greater than the rate of breakdown by MMPs/TIMPs. As plasmin can activate certain MMPs, the pronounced fibrosis in human DMD muscles might thus be related to altered net proteolytic activity in the dystrophic muscles as a result of imbalances in expression and activity of the plasminogen activation/MMP system (Serrano and Muñoz-Cánoves, 2010; Mann et al., 2011). In turn, this imbalance could provoke the aberrant activation of latent TGF-β, thus exacerbating fibrosis development.

A previous study has shown that direct TGF-β immune neutralization reduced collagen accumulation in mdx diaphragm but also resulted in increased inflammation and tissue degeneration, thus precluding direct anti–TGF-β neutralization strategies as a therapeutic option for DMD (Andreetta et al., 2006).

Our study uncovers new ways to interfere upstream and downstream of TGF-β signaling in dystrophic muscle in a more selective manner against fibrosis development and dystrophy progression based on the results obtained with very old dystrophic muscles (which exhibit low levels of PAI-1 and high levels of uPA activity and miR-21). First, down-regulating uPA activity may be a way to limit full TGF-β pericellular activation exclusively in uPA-producing cells, such as stromal fibroblasts within the fibrotic muscle microenvironment. Second, interfering with particular intracellular Smad-mediated responses (such as nongenomic Smad2 responses) in muscle-activated fibroblasts may allow selective targeting of TGF-β profibrotic activities in dystrophic muscle while preserving general TGF-β functions necessary for organism homeostasis. In this direction, a recent study (and our own results) has demonstrated that Smad proteins regulate the maturation of miRs and, in particular, miR-21 in response to TGF-β, via a mechanism independent of their classical genomic functions (Davis et al., 2008). miR-21 is considered an oncomiR based on its strong up-regulation in most human tumors, but it is becoming evident that it may represent a common feature of pathological cell growth or cell stress, as illustrated by their recently reported roles in cardiac and lung diseases by targeting Sprouty2 and Smad7 (Thum et al., 2008; Krichevsky and Gabriely, 2009; Liu et al., 2010), although, in light of a very recent study, miR-21 function in heart remodeling remains controversial (Patrick et al., 2010). Interestingly, we confirmed that the inhibitory Smad, Smad7, but not Sprouty2, was dysregulated in a PAI-1/miR-21–dependent manner in dystrophic muscle (Fig. S5 F), thus providing an amplifying loop for TGF-β activation. Together, our findings clearly implicate miR-21 in skeletal muscle–degenerative fibrotic diseases associated with aging.

New technologies have been implemented to pharmacologically modulate miR functions (Hutvágner et al., 2004; Krützfeldt et al., 2005), favoring the development of alternative therapeutic strategies. Muscle fibrosis reversal in senescent mdx mice (24 mo of age) and in young PAI-$1^{-/-}$ mdx muscle (which resemble older mdx muscle) supports efforts to treat fibrosis in human muscular dystrophies by inactivating miR-21. The capacity of miR-21 to potentially target various downstream effectors of TGF-β signaling in addition to PTEN in fibroblasts (which may include Smad7 or Pdcd4; Thum et al., 2008; Krichevsky and Gabriely, 2009; Liu et al., 2010) might offer a therapeutic advantage to selectively interfere with the complex modulation of fibroblastic cell proliferation and activation in fibrotic muscle while restoring tissue homeostasis, with potentially reduced secondary adverse effects. As muscle fibrosis also represents a major obstacle for successful engraftment of stem cells in dystrophic muscle (Gargioli et al., 2008), targeting miR-21 appears to be an easy-to-test alternative to improve future DMD stem cell therapies in otherwise untreatable individuals.

Materials and methods

Generation of double mutant mice

PAI-1 (serpine-1) knockout male mice 1 were crossed with mdx female mice (Jackson ImmunoResearch Laboratories, Inc.). Male F1 mice were bred with mdx female mice, and their F2 heterozygous (PAI-$1^{+/-}$) male and female offspring were intercrossed. The resulting F3 generation showed the expected Mendelian distribution of PAI-$1^{+/+}$, PAI-$1^{+/-}$, and PAI-$1^{-/-}$ genotypes, all of them in an mdx background. Genotypes were confirmed as previously described (Carmeliet et al., 1993; Carmeliet and Collen, 1994; Suelves et al., 2007). All animal experiments were approved by the Catalan Government Animal Care Committee.

Induction of muscle injury

A muscle laceration model was developed in mice as previously described (Menetrey et al., 1999), with some modifications. In brief, tibialis muscles were cut at 60% of the length from their distal insertion, through 75% of their width and 50% of their thickness, controlling afterward the bleeding with cauterization or simple compression. The mice were sacrificed at different time points after injury (15, 21, or 28 d), and the muscles were frozen in 2-methylbutane precooled in liquid nitrogen and stored at −80°C until analysis. Additionally, skeletal muscle was injured by intramuscular injection of 150 µl of 10–5 M cardiotoxin (CTX; Latoxan) in the tibialis muscle (Suelves et al., 2007). Uninjured muscles were used as reference for time 0. For injection of cytokines in vivo, 50 ng TGF-β1 (recombinant human TGF-β1; R&D Systems) in a volume of 50 µl was injected in the injured muscle. Control RGD peptide (GRGDNP; Enzo Life Sciences) and the cyclic RGD peptide (GpenGRGD; Bachem) were injected i.p. at a dose of 30 mg/Kg every other day during 15 d. For miR treatment in vivo, 5 µg in a volume of 10 µl of either anti–miR-21, miR-21 mimic, or Scramble control oligomiR (Thermo Fisher Scientific) was injected in the injured or dystrophic muscles. Additionally, two anti–miR-21 point mutations, miR-21 U and miR-21 C3 (Ant-miR-21 U/C3), were also used (Zeng and Cullen, 2003). For siRNA treatment in vivo, 5 µg in a volume of 10 µl of either siRNA uPA (Mouse PLAU; Thermo Fisher Scientific) or negative control was injected in the injured or dystrophic muscles. Frequency of oligonucleotide administration and duration of the different treatments for each set of experiments are specified in the corresponding figure legends. Morphological examinations were performed at the indicated days after injury/treatment.

Amiloride treatment

A set of two groups of PAI-$1^{-/-}$ mdx mice of 3 mo of age (10 mice each) was administered amiloride during 15 d in drinking water to deliver 10 mg/Kg/day. In parallel, two groups of 10 mice were administered only vehicle in drinking water. A set of two groups of PAI-$1^{+/+}$ mdx mice of 9 mo of age received in drinking water amiloride or vehicle for 1 mo.

Patient study

Human samples were a gift from J. Colomer (Hospital Sant Joan de Déu, Barcelona, Spain); DMD diagnosis was established on a total absence of dystrophin by immunohistochemistry and confirmed by Western blotting. Muscle samples were obtained by a standard quadriceps muscle biopsy from DMD patients (seven patients between 6 and 12 yr of age) and healthy human controls of similar age (9–15 yr). Histological analysis and characterization of muscle fibrosis were performed similarly to mouse samples, as explained in the next section.

Histological analysis, immunohistochemistry, and image acquisition

Tibialis anterior (TA) or gastrocnemius muscles were isolated and frozen in liquid nitrogen–cooled isopentane or embedded in paraffin. Cryosections (10-µm thickness) were stained with hematoxylin/eosin (H/E) or Sirius red (Sigma-Aldrich). Immunohistochemistry with paraffin-embedded or frozen sections was performed using the following primary antibodies: rabbit polyclonal phospho-Smad2, sheep polyclonal PAI-1 (American Diagnostica Inc.), rabbit polyclonal TGF-β1 (Abcam), rabbit polyclonal collagen type 1 (Millipore), and rabbit polyclonal fibronectin (Abcam). Fibroblasts were detected using the antibodies rabbit polyclonal fibroblast-specific protein–1 (FSP-1; Abcam) and rabbit polyclonal TCF-4 (Cell Signaling Technology; Okada et al., 1997; Zeng and Cullen, 2003; Mathew et al., 2011; Murphy et al., 2011). Labeling of sections with mouse monoclonal primary antibodies was performed using the peroxidase or fluorescein M.O.M. staining kit (Vector Laboratories) according to the manufacturer's instructions. Double immunostaining was performed with sequential addition of each primary and secondary antibody using the appropriate positive and negative controls. Sections were air dried, kept unfixed (Pax7 and embryonic myosin heavy chain) or fixed on 2–4% PFA, washed on PBS, and incubated with primary antibodies according to manufacturer's instructions after blocking for 1 h at room temperature with a high protein–containing solution on PBS (Vector Laboratories). Subsequently, the slides were washed on PBS and incubated with appropriate secondary antibodies and labeling dyes. For immunofluorescence, secondary antibodies were coupled to Alexa Fluor 488 or 568 fluorochromes, and nuclei were stained with DAPI (Invitrogen). After washing, tissue

sections were mounted with VectaShield containing DAPI (Vector Laboratories) or Mowiol.

Digital images were acquired using an upright microscope (DMR6000B; Leica) equipped with a DFC300FX camera for immunohistochemical color pictures or an ORCA-ER camera (Hamamatsu Photonics) for immunofluorescence pictures. HCX PL Fluotar 10×/0.30 NA, 20×/0.50 NA, and 40×/0.75 NA objectives were used. Acquisition was performed using Application or LAS AF software (Leica). Images were composed and edited in Photoshop (CS5; Adobe), in which background was reduced using brightness and contrast adjustments applied to the whole image. Individual fibers were outlined, and their cross-sectional area was determined with the public domain image analysis software ImageJ (National Institutes of Health).

ISH

ISHs were performed in 10-µm cryosections from gastrocnemius muscles using antisense locked nucleic acid (LNA)–modified oligonucleotides (Silahtaroglu et al., 2007). LNA/DNA oligonucleotides contained LNAs at eight consecutive centrally located bases and had the following sequences: LNA-miR-21 5′-TCAACATCAGTCTGATAAGCTA-3′ and LNA-scrambled 5′-CATTAATGTCGGACAACTCAAT-3′. In brief; the sections were dried at room temperature followed by fixation in 4% PFA and by treatment with 10 µg/ml proteinase K. Sections were then blocked with hybridization solution and incubated with FITC-conjugated miR-21 probes or FITC-conjugated control probes (Eurogentec) with a scrambled sequence (Eurogentec). The sections were washed with 0.2× SSC followed by incubation with HRP-conjugated anti-FITC antibody (Roche) overnight. Nuclei were counterstained with hematoxylin.

Characterization of muscle fibrosis

Quantification of collagen content in muscle was performed according to Vidal et al. (2008). In brief, 5–10 cryosections (10-µm thickness) were collected in a tube and sequentially incubated with a solution containing 0.1% Fast green in saturated picric acid, washed with distillated water, incubated with 0.1% Fast green and 0.1% Sirius red in saturated picric acid, washed with distillated water, and gently shaken in a solution of 0.1 M NaOH in absolute methanol (1 vol/1 vol). Absorbance was measured in a spectrophotometer at 540- and 605-nm wavelengths. Total protein and collagen equivalences of the obtained absorbance values were calculated afterward. Histological characterization of muscle fibrosis after Sirius red staining was performed by image analysis quantification as previously described (Vidal et al., 2008). The relative area of the sections occupied by Sirius red staining was obtained on digital pictures of muscle samples processed with ImageJ software after conversion of the original pictures on binary images. Collagen values were expressed as the percentage of the total area of the section occupied by Sirius red staining.

Western blotting analysis

Preparation of cell lysates and Western blotting were performed as described in Perdiguero et al. (2007). In brief, cell lysates were prepared with IP buffer (50 mM Tris-HCl, pH 7.5, 150 mM NaCl, 1% NP-40, 5 mM EGTA, 5 mM EDTA, 20 mM NaF, and 25 mM β-glycerophosphate) supplemented with protease and phosphatase inhibitors (Complete Mini [Roche] and phosphatase inhibitor cocktail [Sigma-Aldrich]). Equal amounts of extracts (50 or 100 µg) were separated by 8 or 10% SDS-PAGE, transferred to nitrocellulose membranes, and detected with primary antibodies against phosphorylated AKT (P-AKT) Ser473, AKT, P-Smad2, Smad2/3, PTEN (Cell Signaling Technology), β-actin, and α-tubulin (Sigma-Aldrich). Secondary anti–rabbit IgG-HRP antibodies (Dako) were used, and HRP was detected using an ECL detection system according to the manufacturer's instructions (GE Healthcare).

Functional performance (Treadmill assay)

The assay was performed using a treadmill apparatus (Treadmill; Panlab) consisting of a motor-driven belt varying in terms of speed (5–150 rpm) and a slope at 10°. At the end of the treadmill, an electrified grid was placed, on which foot shocks (0.6 mA) were administered whenever the mice fell off the belt. The latency to fall off the belt (time of shocks in seconds) and the number of received shocks in consecutive trials with increasing fixed rotational speeds (5, 10, 20, 30, 40, and 50 rpm) with a cutoff period of 1 min per trial were registered. Animals were trained to walk on the treadmill at a constant speed (5 rpm) to obtain baseline values for locomotion in the intact state.

Cell culture and isolation of primary cells

Primary fibroblasts were isolated from mouse diaphragm and cultured as previously described (Vidal et al., 2008). In brief, after dissection from indicated mice, muscles were minced to 1-mm^3 pieces in a sterile Petri dish, and the small pieces were distributed in a 12-well plate containing 0.5 ml DME-F12 with 50% FBS per well. The plates were then incubated at 37°C with 5% CO_2 for 10 d (changing the medium every 2 d) to allow fibroblasts to migrate out of the tissue explants. When cells reached 50% confluence, the minced tissue masses were removed, and fibroblasts were trypsinized and subcultured in 60-mm culture plates. When indicated, primary fibroblasts were stimulated with 10 ng/ml recombinant active TGF-β1 (R&D Systems), 1 mM amiloride (Sigma-Aldrich), 2.5 ng/ml recombinant PAI-1 (American Diagnostica Inc.), and 2 µM wortmannin (Sigma-Aldrich) in the absence or presence of 30 µg/ml of TGF-β–neutralizing antibody (R&D Systems).

Transfections

For miR-21 experiments, Lipofectamine 2000 reagent (Invitrogen) was used to transfect cells with anti–miR-21, miR-21 mimic, or Scramble control oligomiR for 72 h following the manufacturer's instructions. Samples were collected after 72 h of transfections for quantification of miR and protein expression. In some cases, 72 h after transfections, 10 ng/ml of TGF-β1 was added to the cells for an additional 24 h. The same procedure was used to transfect siRNA uPA (Mouse PLAU).

Measurement of uPA and plasmin activities

uPA and plasmin activities were measured indirectly in muscle or cell extracts using the S-2251–based assay. For plasmin activity measurement, the extracts were mixed with a buffer containing 0.1 M Tris-HCl and 2 mM EDTA, pH 7.6, plus 1.6 mM S-2251 as a substrate, and the change in absorbance at 405 nm was measured. For uPA activity, 100 nM plasminogen was added to the mixture. Further details can be found in Suelves et al. (2007).

Quantification of TGF-β1

The protein concentration of active TGF-β1 and total (active plus latent) TGF-β1 levels was quantified by ELISA (Promega) without or with acidification, respectively, following the manufacturer's instructions.

RNA isolation and quantitative RT-PCR

RNA was analyzed by quantitative RT-PCR. Total RNA was isolated from cells or muscle tissue using TriPure reagent (Roche). DNase digestion of 10 µg of RNA was performed using 2 U DNase (TURBO DNA-free; Invitrogen). cDNA was synthesized from 2 µg of total RNA using the First Strand cDNA Synthesis kit (GE Healthcare). PCRs were performed on a LightCycler 480 System using a LightCycler 480 SYBR green I Master (Roche) with specific primers (sequences available in Figs. 1 F, 2 E, 3 [C and G], 5 B, 6 C, S2 B, and S5 [B and F]). The thermocycling conditions used were as follows: an initial step of 10 min at 95°C, 50 cycles of a 15-s denaturation at 94°C, 10 s annealing at 60°C, and a 15-s extension at 72°C. Reactions were run in triplicate, and automatically detected threshold cycle values were compared between samples. Transcripts of the ribosomal protein L7 gene were used as an endogenous normalization control for mouse samples and glyceraldehyde 3-phosphate dehydrogenase for human samples.

Sequences of the primers used for quantitative PCR are as follows: PAI-1, 5′-CAGAGAGCTGCTCTTGGTCGG-3′ and 5′-CAGGTGGACTTCTCAGAGGTGG-3′; collagen I, 5′-GGTATGCTTGATCTGTATCTGC-3′ and 5′-AGTCCAGTTCTTCATTGCATT-3′; TGF-β1, 5′-CTCCACCTGCAAGACCAT-3′ and 5′-CTTAGTTTGGACAGGATCTGG-3′; TIMP-1, 5′-CTTCTGCAATTCCGACCTCGT-3′ and 5′-CCCTAAGGCTTGGAACCCTTT-3′; fibronectin-1 (FN1), 5′-GCGACTCTGACTGGCCTTAC-3′ and 5′-CCGTGTAAGGGTCAAAGCAT-3′; PDGF, 5′-TGAAAGAGGTCCAGGTGAGG-3′ and 5′-CACGGAGGAGAACAAAGACC-3′; α–smooth muscle actin, 5′-TCCCTGGAGAAGAGCTACGA-3′ and 5′-CTTCTGCATCCTGTCAGCAA-3′; Smad 7, 5′-AGCTGGTGTGCTGCAACCCC-3′ and 5′-CAGCATCTGGACAGCCTGCAGT-3′; Sprouty2, 5′-TCCAAGAGATGCCCTTACCCA-3′ and 5′-GCAGACCGTGGAGTCTTTCA-3′; L7, 5′-GAAGCTCATCTATGAGAAGGC-3′ and 5′-AAGACGAAGGAGCTGCAGAAC-3′; human collagen I, 5′-AACCCGAGGTATGCTTGATCT-3′ and 5′-CCAGTTCTTCATTGCATTGC-3′; human TGF-β1, 5′-GGCCAGATCCTGTCCAAGC-3′ and 5′-GTGGGTTTCCACCATTAGCAC-3′; human TIMP-1, 5′-CTTCTGCAATTCCGACCTCGT-3′ and 5′-CCCTAAGGCTTGGAACCCTTT-3′; and human FN1, 5′-GGATGACAAGGAAAATAGCCCTG-3′ and 5′-GAACATCGGTCACTTGCATCT-3′.

Quantification of miR expression

The total RNA including the miR fractions was isolated using the miRNeasy kit (QIAGEN). The quantification of miR-21 (and of miR-146) was performed using Taqman assays for miR (Applied Biosystems) and Taqman Universal

Master Mix (Applied Biosystems). miR levels were quantified using miR-U6B as the housekeeping miR. To analyze miR-21 biogenesis, Pri-miR-21 was determined using the Taqman Pri-miR assays developed by Applied Biosystems.

Statistical analysis

Prism software (GraphPad Software) was used for all statistical analyses. Results from the corresponding time points of each group were averaged and used to calculate descriptive statistics. One-way analysis of variance and Tukey's or Dunnett's post-hoc tests were used on multiple comparisons and all possible pair-wise comparisons among groups at each time point. Data are mean ± SEM. Significance was accepted at $P \leq 0.05$.

Online supplemental material

Fig. S1 (A–D) is related to Fig. 1 and confirms the increased fibrosis and miR-21 expression in aged mdx limb muscles; Fig. S1 (E and F) is related to Fig. 2 and shows the effect of Ant-miR-21 and Mimic-miR-21 in the number of fibroblasts and ECM in lacerated aged and young mdx muscles; Fig. S1 (G and H) is related to Fig. 2 and shows the efficiency of Ant-miR-21 using a point-mutated Ant-miR-21 and an irrelevant miR (miR-146); and Fig. S1 (I and J) is related to Fig. 3 and shows the effect of Ant-miR-21 over TGF-β1 treatment in injured muscle. Fig. S2 (A–C) is related to Fig. 4 and contains uPA and plasmin activities, TGF-β activation, and ECM-related gene expression in lacerated muscles; Fig. S2 D is related to Fig. 4 and shows uPA activity, TGF-β activation, and miR-21 expression in primary fibroblasts; and Fig. S2 E shows the RGD treatment in lacerated muscles. Fig. S3 is related to Fig. 5 and contains functional assays in PAI-$1^{+/+}$ and PAI-$1^{-/-}$ mdx mice and inhibitory uPA treatments in young PAI-$1^{-/-}$ mdx and in aged mdx mice. Fig. S4 is related to Figs. 5 and 6 and contains inhibitory uPA treatments in lacerated PAI-$1^{-/-}$ muscle, PAI-1 expression in fibroblasts in mdx muscle, and fibroblast presence in PAI-$1^{+/+}$ and PAI-$1^{-/-}$ mdx muscles. Fig. S5 is related to Fig. 6 and contains uPA modulatory treatments in cultured PAI-$1^{-/-}$ fibroblasts, a wortmannin effect on PAI-$1^{-/-}$ fibroblast proliferation, and improved muscle recovery in lacerated PAI-$1^{-/-}$ muscle after uPA and miR-21 inhibitory treatments. Online supplemental material is available at http://www.jcb.org/cgi/content/full/jcb.201105013/DC1.

We are indebted to Drs. M. Jardí, V. Ruiz-Bonilla, and V. Lukesova for excellent technical help, all members of our laboratory for helpful discussions, and Dr. J. Martín-Caballero for assistance in animal care.

The authors acknowledge funding from the Ministerio de Ciencia e Innovación (PLE2009-0124, SAF2009-09782, FIS-PS09/01267, and Centro de Investigación Biomédica en Red, Enfermedades Neurodegenerativas), AFM, Fundació La Marató de TV3, Muscular Dystrophy Association, and MYOAGE, OptiStem, and EndoStem (EU-FP7).

Submitted: 3 May 2011
Accepted: 29 November 2011

References

Andreetta, F., P. Bernasconi, F. Baggi, P. Ferro, L. Oliva, E. Arnoldi, F. Cornelio, R. Mantegazza, and P. Confalonieri. 2006. Immunomodulation of TGF-beta 1 in mdx mouse inhibits connective tissue proliferation in diaphragm but increases inflammatory response: Implications for antifibrotic therapy. *J. Neuroimmunol.* 175:77–86. http://dx.doi.org/10.1016/j.jneuroim.2006.03.005

Carmeliet, P., and D. Collen. 1994. Evaluation of the plasminogen/plasmin system in transgenic mice. *Fibrinolysis*. 8:269–276. http://dx.doi.org/10.1016/0268-9499(94)90725-0

Carmeliet, P., L. Kieckens, L. Schoonjans, B. Ream, A. van Nuffelen, G. Prendergast, M. Cole, R. Bronson, D. Collen, and R.C. Mulligan. 1993. Plasminogen activator inhibitor-1 gene-deficient mice. I. Generation by homologous recombination and characterization. *J. Clin. Invest.* 92: 2746–2755. http://dx.doi.org/10.1172/JCI116892

Davis, B.N., A.C. Hilyard, G. Lagna, and A. Hata. 2008. SMAD proteins control DROSHA-mediated microRNA maturation. *Nature*. 454:56–61. http://dx.doi.org/10.1038/nature07086

Deconinck, N., and B. Dan. 2007. Pathophysiology of duchenne muscular dystrophy: Current hypotheses. *Pediatr. Neurol.* 36:1–7. http://dx.doi.org/10.1016/j.pediatrneurol.2006.09.016

Flier, S.N., H. Tanjore, E.G. Kokkotou, H. Sugimoto, M. Zeisberg, and R. Kalluri. 2010. Identification of epithelial to mesenchymal transition as a novel source of fibroblasts in intestinal fibrosis. *J. Biol. Chem.* 285:20202–20212. http://dx.doi.org/10.1074/jbc.M110.102012

Gargioli, C., M. Coletta, F. De Grandis, S.M. Cannata, and G. Cossu. 2008. PlGF-MMP-9-expressing cells restore microcirculation and efficacy of cell therapy in aged dystrophic muscle. *Nat. Med.* 14:973–978. http://dx.doi.org/10.1038/nm.1852

George, S.J., J.L. Johnson, M.A. Smith, G.D. Angelini, and C.L. Jackson. 2005. Transforming growth factor-beta is activated by plasmin and inhibits smooth muscle cell death in human saphenous vein. *J. Vasc. Res.* 42:247–254. http://dx.doi.org/10.1159/000085657

Hayashida, T. 2010. Integrins modulate cellular fibrogenesis at multiple levels; Regulation of TGF-β signaling. *Endocr. Metab. Immune Disord. Drug Targets*. 10:302–319.

Howell, J.E., and R.J. McAnulty. 2006. TGF-beta: Its role in asthma and therapeutic potential. *Curr. Drug Targets*. 7:547–565. http://dx.doi.org/10.2174/138945006776818692

Hutvágner, G., M.J. Simard, C.C. Mello, and P.D. Zamore. 2004. Sequence-specific inhibition of small RNA function. *PLoS Biol.* 2:E98. http://dx.doi.org/10.1371/journal.pbio.0020098

Krichevsky, A.M., and G. Gabriely. 2009. miR-21: A small multi-faceted RNA. *J. Cell. Mol. Med.* 13:39–53. http://dx.doi.org/10.1111/j.1582-4934.2008.00556.x

Krützfeldt, J., N. Rajewsky, R. Braich, K.G. Rajeev, T. Tuschl, M. Manoharan, and M. Stoffel. 2005. Silencing of microRNAs in vivo with 'antagomirs'. *Nature*. 438:685–689. http://dx.doi.org/10.1038/nature04303

Liu, G., A. Friggeri, Y. Yang, J. Milosevic, Q. Ding, V.J. Thannickal, N. Kaminski, and E. Abraham. 2010. miR-21 mediates fibrogenic activation of pulmonary fibroblasts and lung fibrosis. *J. Exp. Med.* 207:1589–1597. http://dx.doi.org/10.1084/jem.20100035

Liu, X., H. Hu, and J.Q. Yin. 2006. Therapeutic strategies against TGF-beta signaling pathway in hepatic fibrosis. *Liver Int.* 26:8–22. http://dx.doi.org/10.1111/j.1478-3231.2005.01192.x

Lluís, F., J. Roma, M. Suelves, M. Parra, G. Aniorte, E. Gallardo, I. Illa, L. Rodríguez, S.M. Hughes, P. Carmeliet, et al. 2001. Urokinase-dependent plasminogen activation is required for efficient skeletal muscle regeneration in vivo. *Blood*. 97:1703–1711. http://dx.doi.org/10.1182/blood.V97.6.1703

Ludbrook, S.B., S.T. Barry, C.J. Delves, and C.M. Horgan. 2003. The integrin alphavbeta3 is a receptor for the latency-associated peptides of transforming growth factors beta1 and beta3. *Biochem. J.* 369:311–318. http://dx.doi.org/10.1042/BJ20020809

Mann, C.J., E. Perdiguero, Y. Kharraz, S. Aguilar, P. Pessina, A.L. Serrano, and P. Muñoz-Cánoves. 2011. Aberrant repair and fibrosis development in skeletal muscle. *Skelet. Muscle*. 1:21. http://dx.doi.org/10.1186/2044-5040-1-21

Mathew, S.J., J.M. Hansen, A.J. Merrell, M.M. Murphy, J.A. Lawson, D.A. Hutcheson, M.S. Hansen, M. Angus-Hill, and G. Kardon. 2011. Connective tissue fibroblasts and Tcf4 regulate myogenesis. *Development*. 138: 371–384. http://dx.doi.org/10.1242/dev.057463

Medina, P.P., M. Nolde, and F.J. Slack. 2010. OncomiR addiction in an in vivo model of microRNA-21-induced pre-B-cell lymphoma. *Nature*. 467:86–90. http://dx.doi.org/10.1038/nature09284

Menetrey, J., C. Kasemkijwattana, F.H. Fu, M.S. Moreland, and J. Huard. 1999. Suturing versus immobilization of a muscle laceration. A morphological and functional study in a mouse model. *Am. J. Sports Med.* 27:222–229.

Murphy, M.M., J.A. Lawson, S.J. Mathew, D.A. Hutcheson, and G. Kardon. 2011. Satellite cells, connective tissue fibroblasts and their interactions are crucial for muscle regeneration. *Development*. 138:3625–3637. http://dx.doi.org/10.1242/dev.064162

Nunes, I., R.L. Shapiro, and D.B. Rifkin. 1995. Characterization of latent TGF-beta activation by murine peritoneal macrophages. *J. Immunol.* 155: 1450–1459.

Odekon, L.E., F. Blasi, and D.B. Rifkin. 1994. Requirement for receptor-bound urokinase in plasmin-dependent cellular conversion of latent TGF-β to TGF-β. *J. Cell. Physiol.* 158:398–407. http://dx.doi.org/10.1002/jcp.1041580303

Okada, H., T.M. Danoff, R. Kalluri, and E.G. Neilson. 1997. Early role of Fsp1 in epithelial-mesenchymal transformation. *Am. J. Physiol.* 273:F563–F574.

Pan, X., Z.X. Wang, and R. Wang. 2011. MicroRNA-21: A novel therapeutic target in human cancer. *Cancer Biol. Ther.* 10:1224–1232.

Patrick, D.M., R.L. Montgomery, X. Qi, S. Obad, S. Kauppinen, J.A. Hill, E. van Rooij, and E.N. Olson. 2010. Stress-dependent cardiac remodeling occurs in the absence of microRNA-21 in mice. *J. Clin. Invest.* 120:3912–3916. http://dx.doi.org/10.1172/JCI43604

Pedroja, B.S., L.E. Kang, A.O. Imas, P. Carmeliet, and A.M. Bernstein. 2009. Plasminogen activator inhibitor-1 regulates integrin alphavbeta3 expression and autocrine transforming growth factor beta signaling. *J. Biol. Chem.* 284:20708–20717. http://dx.doi.org/10.1074/jbc.M109.018804

Perdiguero, E., V. Ruiz-Bonilla, L. Gresh, L. Hui, E. Ballestar, P. Sousa-Victor, B. Baeza-Raja, M. Jardí, A. Bosch-Comas, M. Esteller, et al. 2007. Genetic analysis of p38 MAP kinases in myogenesis: Fundamental role of p38alpha in abrogating myoblast proliferation. *EMBO J.* 26:1245–1256. http://dx.doi.org/10.1038/sj.emboj.7601587

Serrano, A.L., and P. Muñoz-Cánoves. 2010. Regulation and dysregulation of fibrosis in skeletal muscle. *Exp. Cell Res.* 316:3050–3058. http://dx.doi.org/10.1016/j.yexcr.2010.05.035

Silahtaroglu, A.N., D. Nolting, L. Dyrskjøt, E. Berezikov, M. Møller, N. Tommerup, and S. Kauppinen. 2007. Detection of microRNAs in frozen tissue sections by fluorescence in situ hybridization using locked nucleic acid probes and tyramide signal amplification. *Nat. Protoc.* 2:2520–2528. http://dx.doi.org/10.1038/nprot.2007.313

Stedman, H.H., H.L. Sweeney, J.B. Shrager, H.C. Maguire, R.A. Panettieri, B. Petrof, M. Narusawa, J.M. Leferovich, J.T. Sladky, and A.M. Kelly. 1991. The mdx mouse diaphragm reproduces the degenerative changes of Duchenne muscular dystrophy. *Nature*. 352:536–539. http://dx.doi.org/10.1038/352536a0

Suelves, M., R. López-Alemany, F. Lluís, G. Aniorte, E. Serrano, M. Parra, P. Carmeliet, and P. Muñoz-Cánoves. 2002. Plasmin activity is required for myogenesis in vitro and skeletal muscle regeneration in vivo. *Blood*. 99:2835–2844. http://dx.doi.org/10.1182/blood.V99.8.2835

Suelves, M., B. Vidal, V. Ruiz, B. Baeza-Raja, A. Diaz-Ramos, I. Cuartas, F. Lluis, M. Parra, M. Jardi, R. Lopez-Alemany, et al. 2005. The plasminogen activation system in skeletal muscle regeneration: Antagonistic roles of urokinase-type plasminogen activator (uPA) and its inhibitor (PAI-1). *Front. Biosci.* 10:2978–2985. http://dx.doi.org/10.2741/1754

Suelves, M., B. Vidal, A.L. Serrano, M. Tjwa, J. Roma, R. López-Alemany, A. Luttun, M.M. de Lagrán, A. Díaz-Ramos, M. Jardí, et al. 2007. uPA deficiency exacerbates muscular dystrophy in *MDX* mice. *J. Cell Biol.* 178:1039–1051. http://dx.doi.org/10.1083/jcb.200705127

Thum, T., C. Gross, J. Fiedler, T. Fischer, S. Kissler, M. Bussen, P. Galuppo, S. Just, W. Rottbauer, S. Frantz, et al. 2008. MicroRNA-21 contributes to myocardial disease by stimulating MAP kinase signalling in fibroblasts. *Nature*. 456:980–984. http://dx.doi.org/10.1038/nature07511

Varga, J., and B. Pasche. 2009. Transforming growth factor beta as a therapeutic target in systemic sclerosis. *Nat Rev Rheumatol*. 5:200–206. http://dx.doi.org/10.1038/nrrheum.2009.26

Vidal, B., A.L. Serrano, M. Tjwa, M. Suelves, E. Ardite, R. De Mori, B. Baeza-Raja, M. Martínez de Lagrán, P. Lafuste, V. Ruiz-Bonilla, et al. 2008. Fibrinogen drives dystrophic muscle fibrosis via a TGFbeta/alternative macrophage activation pathway. *Genes Dev.* 22:1747–1752. http://dx.doi.org/10.1101/gad.465908

Worthington, J.J., J.E. Klementowicz, and M.A. Travis. 2011. TGFβ: A sleeping giant awoken by integrins. *Trends Biochem. Sci.* 36:47–54. http://dx.doi.org/10.1016/j.tibs.2010.08.002

Yee, J.A., L. Yan, J.C. Dominguez, E.H. Allan, and T.J. Martin. 1993. Plasminogen-dependent activation of latent transforming growth factor beta (TGF beta) by growing cultures of osteoblast-like cells. *J. Cell. Physiol.* 157:528–534. http://dx.doi.org/10.1002/jcp.1041570312

Zeng, Y., and B.R. Cullen. 2003. Sequence requirements for micro RNA processing and function in human cells. *RNA*. 9:112–123. http://dx.doi.org/10.1261/rna.2780503

Zhou, L., and H. Lu. 2010. Targeting fibrosis in Duchenne muscular dystrophy. *J. Neuropathol. Exp. Neurol.* 69:771–776. http://dx.doi.org/10.1097/NEN.0b013e3181e9a34b